Microglia cell number, density, and morphology classification at postnatal day 10 in dentate gyrus of female and male C57BL/6J mice

Danielle Guez-Barber[1,2,a], Lorianna M. Colon[3,a], Dana Raphael[4], Max A. Wragan[4], Sanghee Yun[2,3], Amelia J. Eisch[3,5]*

[1]Division of Neurology, The Children's Hospital of Philadelphia (CHOP), Philadelphia, PA, USA, 19104
[2]University of Pennsylvania Perelman School of Medicine, Philadelphia, PA, USA, 19104
[3]Department of Anesthesiology and Critical Care Medicine, CHOP Research Institute, Philadelphia, PA, USA, 19104
[4]School of Arts and Sciences, University of Pennsylvania, Philadelphia, PA, USA, 19104
[5]Department of Neuroscience, University of Pennsylvania Perelman School of Medicine, Philadelphia, PA, USA, 19104

[a]These authors contributed equally to this work
*Correspondence: eischa@chop.edu

Keywords: sex differences, development, Iba1, immunohistochemistry, stereology, hippocampus

Pre-Submission Author Contributions (for details and explanations see CRediT):
Listed in alphabetical order by last name
Conceptualization: DGB, AJE, SY
Data curation: DGB, LMC, AJE, MW
Formal Analysis: AJE,SY
Funding acquisition: DGB, AJE
Investigation: DGB, LMC, DR, MW
Methodology: DGB, LMC, MW
Project administration: DGB, AJE
Resources: AJE, DGB
Software: --
Supervision: DGB, AJE, SY
Validation: LMC, DR
Visualization: DGB, LMC, AJE, DR, MW, SY
Writing, original draft: DGB, LMC, AJE, DR, MW
Writing, review & editing: DGB, LMC, AJE, SY

ABSTRACT

Microglia maintain normal brain function and support the brain's response to disease and injury. The hippocampus is an area of focus for microglial study due to its central role in many behavioral and cognitive functions. Interestingly, microglia and related cells are distinct in female vs. male rodents, even in early life. Indeed, postnatal day (P)-dependent sex differences in number, density, and morphology of microglia-like cells have been reported in certain hippocampal subregions at specific ages. However, sex differences in hippocampal microglia have not been examined in the P10 mouse hippocampus. In addition, a key subregion of the hippocampus — the dentate gyrus and its hilar region and molecular layer — has not yet been assessed for sex differences in microglia at P10. To address these knowledge gaps, three measures were collected in the dentate gyrus Hilus and Molecular layer in female and male C57BL/6J mice: number of Iba1+ cells (via stereology), density of Iba1+ cells (via stereology), and density of Iba1+ cells (via sampling). We then classified Iba1+ cell morphology to generate a total number of each cell type (percentage of each cell type via sampling multiplied by cell number via stereology). Analysis of total Iba1+ number, Iba1+ cell density, and morphology type shows no difference between female and male mice in either the Molecular layer or the Hilus at P10. This understudied but important postnatal time point — a rodent developmental time point translationally relevant to human term gestation — fills a key knowledge gap. The data presented here from healthy P10 female and male mice will be useful for research on the role of microglia in injury models. Our demonstration of no sex difference in Iba1+ cells in P10 hippocampal dentate gyrus using two different commonly employed methodologies (sampling and stereology) provides a baseline from which to interpret microglia changes seen after injury.

HIGHLIGHTS

- Sex differences in Iba1+ cells were assessed in the dentate gyrus (DG) of P10 mice
- Iba1+ cells were assessed in microglia-rich DG areas: the Molecular layer and Hilus
- A stereology approach showed no sex difference in DG Iba1+ number or density
- A sampling approach showed no sex difference in DG Iba1+ cell morphology
- In our measures of cell number, density and morphology, there were no sex differences in Iba1+ cells in P10 mice DG

1. INTRODUCTION

Microglia are brain immune cells, but their functions go far beyond their classical role as “trash collectors”. Microglia maintain normal brain function by clearing debris, pruning synapses, regulating neurogenesis, and even regulating cognition and mood-relevant behavior supported by brain regions like the hippocampus [1–8]. Microglia also support the brain’s response to disease and injury [1,9–11]. Interestingly, microglia are distinct in female vs. male rodents, even in early life [12–16]. In the hippocampus, a brain region whose development continues well into the postnatal period, there are sex-, postnatal day (P)-, and hippocampal subregion-dependent differences in number, density, and morphology of microglia [17–20]. There are disagreements in the literature about the directionality of sex differences in early life microglia [16,17,19]. Nevertheless, these studies agree that there is a transition sometime between P4 and P28 when the directionality of sex differences in microglial measures flips. These studies did not assess P10 which neuroanatomically correlates with full term gestation in humans [21], making it a useful time point for many translationally-relevant neurobiological processes. Therefore, sex differences in hippocampal microglia merit examination in the P10 mouse dentate gyrus.

To address this knowledge gap, we collected the following information from the dentate gyrus of female and male P10 mice: number of Iba1+ cells via stereology, density of Iba1+ cells via stereology, density of Iba1+ cells via sampling, and Iba1+ cell morphology (number * density). This information was collected from two dentate gyrus subregions rich with Iba1+ cells: the Molecular layer (Mol) and Hilus. We used both stereology and sampling approaches to fill these knowledge gaps since separate publications using either approach alone has yielded results that are discrepant in some measures across publications [17,18,20,22–25]. The resulting data are important as they examine sex differences in Iba1+ microglia in the mouse hippocampus at P10, an understudied but important postnatal timepoint.

2. METHODS

2.1 Animals

Pregnant multiparous adult female C57BL/6J mice (~12 weeks old) were shipped from Jackson Laboratory (stock #000664) on embryonic day 14 (E14). Dams were individually-housed in a HEPA-filtered, closed airflow vivarium rack (Lab Products Inc., Enviro-Gard™ III) under a normal 12:12-hour light-dark cycle (06:00 on, 18:00 off) with *ad libitum* access to food (standard rodent chow, Lab Diets 5015 #0001328) and water. The AAALAC-accredited facility at the Children’s Hospital of Philadelphia (CHOP) Research Institute is temperature- (22°C) and humidity-controlled (30-70%). Mouse pups were kept in the same cage as the dam and their littermates following birth. Pups from 4 litters from 4 distinct dams were used for this P10 analysis (pups: 11 females, 9 males). Mice were weighed once prior to tissue collection at P10. All mice were cared for in compliance with protocols approved by the Institutional Animal Care and Use Committee at CHOP and guidelines established by the NIH’s *Guide for the Care and Use of Laboratory Animals.* Our scientific reporting adheres to the ARRIVE 2.0 guidelines [26].

2.2 Brain collection and tissue preparation

Mice were sexed prior to brain collection based on anogenital distance and gonadal appearance. Mice were euthanized on P10 via live decapitation using sterilized, surgical scissors in compliance with NIH guidelines for euthanasia of rodent neonates. Once extracted from the skull, brains were fixed for 72 hours (h) at room temperature (RT) in 4% paraformaldehyde (PFA). Following two PFA

changes (one/day), brains were cryoprotected via placement in 30% sucrose in 0.1 M PBS. Forty µm coronal sections at 200 µm intervals through the anterior hippocampus were collected on a freezing microtome (Leica SM 2000 R) and stored in 1xPBS with 0.01% sodium azide at 4°C until processing for immunohistochemistry (IHC).

2.3 IHC

IHC was performed as previously described [27,28]. Brain sections were mounted onto charged slides (Thermo Fisher Scientific, #12-550-15) and left to dry for 1-2 h prior to IHC. Sections underwent antigen retrieval (0.01 M citric acid, pH 6.0, 100°C, 15 min) followed by RT washes in 1xPBS; all subsequent steps also occurred at RT. Non-specific protein binding was blocked via incubation with 3% Normal Donkey Serum (NDS) and 0.3% TritonX-100 in 1xPBS for 60 minutes (min). Following pretreatment and blocking steps, sections were incubated overnight with rabbit-anti-Iba1 (1:500; Wako Chemicals, #019-19741) in a carrier of 3% NDS and 0.3% Tween-20 in 1xPBS. Eighteen hours later, sections were rinsed with 1xPBS prior to incubation with biotinylated donkey-anti-rabbit IgG (1:200; Jackson ImmunoResearch Laboratories, #711-065-152) in 1.5% NDS. After washing with 1xPBS, endogenous peroxidase activity was inhibited via incubation with 0.3% hydrogen peroxide in 1xPBS for 30 min. Following an additional set of 1xPBS washes, slides were incubated with an avidin-biotin complex (ABC Elite, Vector Laboratories, #PK-6100) for 90 min. Slides were washed with 1xPBS and immunoreactive cells were visualized via incubation with metal-enhanced diaminobenzidine (Thermo Fisher Scientific, #34065) for 11-12 min. Slides were counterstained via Fast Red (Vector Laboratories, #H3403), dehydrated in a series of increasing ethanol concentrations and Citrosolv, and coverslipped with DPX (Thermo Fisher Scientific, #50-980-370).

2.4 Stereological counting procedure

To determine the total number of Iba1+ cells in dentate gyrus (DG) subregions, we used unbiased stereology via the optical fractionator probe (Stereo Investigator, MBF Bioscience, Williston, VT, USA). All stereology data were collected by a person blinded to sex of the mouse. We first delineated the Mol and Hilus using a low-power 5x objective (Zeiss AxioImager M2 microscope) on coronal sections through the first 2400µm of the DG (**Fig 1A**) beginning at -1.35mm from bregma, and using a section sampling fraction (ssf) of 1/6 (**Fig 1B**). To delineate the Hilus, a line was drawn from the tip of the infrapyramidal blade to the tip of the suprapyramidal blade of the DG and around the inner border of the GCL. To delineate the Mol, following the trajectory of the Hilus, a line was extended up from the edge of the suprapyramidal blade to the hippocampal fissure, across the outer border of the GCL, and along the border of the infrapyramidal blade. To count Iba1+ cells we used a high-power 40x objective (Zeiss AxioImager M2 microscope). The counting frame was set to 60x 60µm for the Hilus and 50 x 50µm for Mol. The height of the dissector was 10µm and the size of the sampling grid for both regions of interest were set at 125 x 125µm. The counting frame, dissector height, and grid size were tested during a pilot study and chosen to achieve a Schaeffer coefficient error of 0.01 or less, which has been accepted as the standard level of error for stereological estimates [29,30]. The section thickness after staining was assessed through the z focal plane at each counting site, and the total cell number estimate was based on the number weighted section thickness. All Iba1+ cell bodies that came into focus within the counting frame or crossing acceptance lines without touching rejection lines [31] and met our criteria for size (~10µm), color (even staining), and shape (round, stout, thick or thin) were counted and added to the total sample of markers. The total estimated population using number weighted section thickness was generated by the optical fractionator probe; this value represents the total number Iba1+ cells within the first 2400µm of the DG. In cases where a section of tissue was damaged or folded in the region of interest, the missing section tool in the optical

fractionator probe was utilized and the estimate adjusted by missing section fraction value (Stereo Investigator), which corrects for missing or damaged sections, was used to provide an unbiased measure of the total number of Iba1+ cells. Of the 399 sections analyzed (200 Mol section, 199 Hilus sections) the missing section tool was utilized on a total of 13 sections.

2.5 Iba1+ cell density determination via stereology

To determine the density of Iba1+ cells in the DG we first assessed volume using the Cavalieri estimator probe (Stereo Investigator). The section cut thickness was defined at 40μm and the grid spacing between reference points was set at 100μm. After generating an estimated volume of Mol and Hilus for each animal, we divided the total number of Iba1+ cells for each animal (determined via stereology optical fractionator probe) by the total volume within the Hilus and Mol to generate a density estimate.

2.6 Iba1+ cell density determination via sampling

Images from immunostained sections were captured in bright-field light microscopy using an Olympus BX51 microscope with a 40x/0.9NA objective and an Olympus DP74 camera (widescreen aspect ratio, 16:10). For cell density data collection, a single section in the anterior hippocampus was selected and all Iba1+ cells in the bilateral Hilus and Mol of each photomicrograph were evaluated. For each mouse, a total of four 400x images were collected (2 hippocampal subregions from each hemisphere in the anterior hippocampus, -2.05 mm from bregma), similar to prior work [18,24]. Criteria for inclusion as an Iba1+ cell were a consistently-labeled soma easily distinguishable from the counterstain and the presence of an entire cross-sectional view through the soma in the focal plane captured in the photomicrograph. Photomicrographs were collected by a person blinded to sex. Guidelines for taking photomicrographic images of the DG subregions (Mol, Hilus; **Fig 2A-B**) were established to enable anatomical matching of subregions across hemispheres and mice and to reduce inter-person variation in taking photomicrographs. These guidelines were as follows: Mol: the outer Mol near the dentate gyrus crest was positioned in the bottom and lateral corner of the image. Hilus: the DG crest was placed in the lateral and central screen such that the Hilus extended into the middle of the image. After photomicrographs were collected, a region of interest (ROI) was drawn on each image using FIJI by an observer blinded to sex. This ROI ensured the appropriate regions would be analyzed (e.g. Mol) and other regions that may be in the image would be excluded (**Fig 2C-D**), and enabled quantification of total pixels within each ROI. For analysis, ROI areas (in pixels) were converted to um^2 based on 1 pixel=0.0231 um^2. The photomicrographs for each subregion were annotated to indicate each Iba1+ cell that was counted and its morphology classification. This enabled a permanent record of the data collection and also allowed data collection validation as additional observers of the original, non-annotated photomicrographs could compare their results with the annotated versions. Iba1+ cell count for one hemisphere for each of the DG subregions was divided by the area of the ROI to generate an Iba1+ cell density for that hemisphere (**Fig 2E-F**). Density values for each hemisphere were averaged such that each mouse was represented by one density value for each subregion.

2.7 Image collection and preparation for morphology analysis

Each Iba1+ cell examined in the sampling approach was simultaneously placed into one of four previously-published morphology categories [17,20,32–34]: Round or ameboid (round-ish soma, no processes), Stout (round-ish soma, short process), Thick (irregular soma with few, thick processes), or Thin (irregular soma with multiple thin processes; **Fig 3A-D**). The number of cells in each category was transformed into a percentage based on the total number of Iba1+ cells classified in the bilateral anterior hippocampus. A percentage for each of the four categories (Round, Stout, Thick, and Thin)

was generated for each hemisphere in each subregion. The four percentages from hemisphere subregions were averaged with the other hemisphere subregion percentage, such that each mouse subregion was represented by four category percentages. The percentage of each morphological cell type in the Hilus and Mol were multiplied by the total number of cells generated via stereology to produce a single value for total number of cells by each morphological classification (**Fig 3E-F**),

2.8 Data analysis and statistics

Sex of the mice was masked until data collection was complete. Data were analyzed via Prism 9 (Graphpad). Normality tests via group distribution were first assessed by the D'Agostino and Pearson test which revealed groups to be normally distributed. Normally-distributed Iba1+ total cell number via stereology and cell density measures via sampling and stereology for Hilus and Mol were next tested via t-test for an effect of sex. Normally-distributed Iba1+ morphology classification for each subregion was tested via 2-way ANOVA (main effects: Sex [Male, Female] X Morphology [Round, Stout, Thick, Thin]). Data are expressed as mean +/- SEM and $\alpha = 0.05$.

3. RESULTS

*3.1 Stereological analysis showed Iba1+ cell **number** in the Hilus and Mol were not different between female and male mice at P10.* Iba1+ cells were evident in both the Hilus and Mol of all male and female mice examined. The number of Iba1+ cells in male and female mice were quantified via unbiased stereology. Unpaired t-test revealed no sex difference in total number of cells within the first 2400um of the dentate gyrus in either the Hilus [$t(18) = 0.067$; $p>0.05$] (**Fig 1C**) or Mol [$t(18) = 0.154$; $p>0.05$] (**Fig 1D**).

*3.2 Stereological assessment of Iba1+ cell **density** in and total **volume** of the Hilus and Mol were also not different between female and male mice at P10.* The density of Iba1+ cells in male and female mice were quantified via stereology using the Cavalieri tool. Unpaired t-test revealed no sex difference in density of Iba1+ cells within the the dentate gyrus in either the Hilus [$t(18) = 0.271$; $p>0.05$] (**Fig 1E**) or Mol [$t(18) = 0.3402$; $p>0.05$] (**Fig 1F**). Unpaired t-test revealed no sex difference in total volume of the dentate gyrus in either the Hilus [$t(18) = 0.5438$; $p>0.05$] (**Fig 1G**) or Mol [$t(18) = 0.3150$; $p>0.05$] (**Fig 1H**).

*3.3 **Sampling** assessment of Iba1+ cell **density** in the Hilus and Mol were not different between female and male mice at P10*. Following the guidelines for selecting subregion areas to consistently sample across mice **(Fig 2A-E)**, Iba1+ cell densities were quantified via sampling. Unpaired t-test revealed no sex difference in cell density in either the Hilus [$t(18) = 1.012$; $p>0.05$] **(Fig 2F)** or Mol [$t(18) = 0.259$; $p>0.05$] **(Fig 2G)**.

*3.4 Classification of Iba1+ cell **morphology** in the Hilus and Mol were not different between female and male mice at P10*. In each subregion, Iba1+ Thick and Thin cells were evident, while Iba1+ Round and Stout cells were far more rare **(Fig 3E-F)**. A two-way ANOVA Sex [Male, Female] X Morphology [Round, Stout, Thick, Thin]) revealed no sex-dependent effects in regard to Iba1+ cell morphology classification in either the Hilus [$F(3,72) = 1.032$; $p>0.05$] **(Fig 3E)** or Mol [$F(3,72) = 2.162$; $p>0.05$] **(Fig 3F)**.

4. DISCUSSION

Employing two separate commonly used techniques (stereology and sampling [17,18,20,22–25]) we find no difference in total Iba1+ cell number or cell density between female and male mice at P10 in dentate gyrus Hilus or Mol. We also found no sex differences in the percentage of morphological cell types (Round, Stout, Thick, and Thin). The lack of sex-dependent difference in Iba1+ cell number or density in the P10 dentate gyrus is interesting in the context of prior work. In rat dentate gyrus, female and male microglia differ in early development: at P4 when most microglia have an immature morphology, males have more amoeboid microglia than females, but by P30 when most microglia have mature morphology, females have more thick microglia than males [17]. In this comprehensive study, Schwartz, *et al.,* examined many timepoints from embryonic day 17 through adulthood P60, but did not evaluate timepoints between P4 and P30 when this transition occurs. Our work here showing no sex-dependent difference in Iba1+ cell number, density, or morphology in the dentate gyrus at P10 may represent this “switch”. Other studies found that female mice have increased Iba1 volume at P8 relative to males, but this is decreased at P28 [19]. They conclude that hippocampal microglial development occurs earlier in females than males; this conclusion is supported by another study that uses an entirely different transcriptome approach [16]. When there are no sex differences in cell number, there can still be sex differences in gene expression patterns and other important phenotypes [20,35].

Our morphology classification data are similarly interesting, particularly in that there is a greater percentage of Thick and Thin Iba1+ cells in the Mol and Hilus in both sexes at P10. This likely reflects the “age” or maturity of the microglia, with Round microglia (ameboid, no processes) considered relatively “less mature” than ramified Thin microglia [17]. Notably, in the adult rodent, similar microglia morphology categories have been used as a gradient to reflect the degree of “activation” of microglia. However, there has been a recent call to reevaluate the nomenclature used to describe and define microglia [36]. This modern view argues that terms such as “activation” or “resting” do not adequately capture the highly dynamic nature of microglial cell states as these states (and transitions) can be influenced by age, sex, health or disease, and context.

There are limitations of this study. First, we are presuming that Iba1+ cells are microglia. However, Iba1 is expressed in the brain in several cell populations: brain-resident yolk-sac derived microglia, infiltrating peripheral monocyte-derived macrophages, as well as border-associated macrophages [36,37]. Although some of the Iba1+ cells analyzed here may be one of the latter two categories, prior research suggests this is a very low percentage, particularly in the uninjured brain[25,38]. Definitive assessment of the Iba1+ cells analyzed in our work as microglia vs. infiltrating macrophages will require co-labeling with markers to distinguish microglia from infiltrating peripheral macrophages [25,39]. Second, the pups used for this study came from timed pregnant dams who were delivered to our facility during pregnancy. It remains to be seen if pups from dams bred in-house will have similar differences in morphology classification as presented here.

In sum, here we show that there is no difference in Iba1+ cell number, density, or morphology between female and male mice in the dentate gyrus at P10. Because P10 is a rodent developmental time point translationally relevant to human term gestation [21], this fills a key knowledge gap. The data presented here from healthy P10 female and male mice will be useful for research on the role of microglia in injury models, which often do not consider baseline microglia values. Our demonstration

of no sex difference in Iba1+ cells in P10 hippocampal dentate gyrus provides a baseline from which to interpret microglia changes seen after injury.

5. Funding and acknowledgements

DGB is supported by “Remapping the Clinical Neurosciences through Translation and Innovation Training” (2T32NS091008; co-PIs: Jensen, Aguirre), several avenues of support from the Children’s Hospital of Philadelphia (CHOP) Research Institute (the Supplemental Support for Clinicians to Pursue Research Training in Neuroscience, a Foerderer Award for Excellence, a K-Readiness Faculty Pilot Program Award), the Alavi-Dabiri Postdoctoral Fellowship Award from CHOP’s Intellectual and Developmental Disabilities Research Center, the CHOP Division of Neurology, and the Child Neurologist Career Development Program CNCDP-K12 (NS098482, PI: Schlaggar). LMC is supported by the CHOP Postdoctoral Diversity Fellowship. HMP and MW were supported by the University of Pennsylvania’s (Penn) Center for Undergraduate Research and Fellowships (CURF). DR was also supported by CURF as well as by funds from being named a Penn Department of Neuroscience Scholar. SY is supported by a 2019 NARSAD Young Investigator Grant from the Brain and Behavior Research Foundation, a 2020 University of Pennsylvania Undergraduate Research Foundation grant, an NIH R01 grant (NS088555-05, PI: AM Stowe), a 2021 NASA HERO grant (80NSSC21K0814), and a Foerderer Award for Excellence from CHOP. AJE and this work are also supported by Bridge Funding from the CHOP Research Institute, an NIH R01 grant (NS088555-05, PI: AM Stowe), and a research grant from the Peter F. McManus Charitable Trust. We are indebted to Sharon Xie for biostatistical guidance, F. Chris Bennett, Graham Peet and Mariko Bennett for microglia imaging advice and discussions, Margaret McCarthy for discussions on microglia and sex differences in early life, and Kelly Jordan-Sciutto’s group for permission to use their imaging set-up in the initial stage of this project. Thanks to many Eisch Lab members and colleagues for helpful discussions and guidance, in particular Lyles R. Clark and Fred C. Kiffer, and to Ruthie E. Wittenberg for input and editing. We thank Haley M. Phillips and Kira Lu for preliminary help with early data analysis.

Declaration of Interest

None of the authors have any conflict of interest to declare.

Data Availability Statement

An electronic copy of all experimental data will be made available upon reasonable written request.

REFERENCES

[1] A. Sierra, O. Abiega, A. Shahraz, H. Neumann, Janus-faced microglia: beneficial and detrimental consequences of microglial phagocytosis, Front. Cell. Neurosci. 7 (2013) 6.

[2] S. Hong, L. Dissing-Olesen, B. Stevens, New insights on the role of microglia in synaptic pruning in health and disease, Curr. Opin. Neurobiol. 36 (2016) 128–134.

[3] Y. Wu, L. Dissing-Olesen, B.A. MacVicar, B. Stevens, Microglia: Dynamic Mediators of Synapse Development and Plasticity, Trends Immunol. 36 (2015) 605–613.

[4] K.M. Lenz, L.H. Nelson, Microglia and Beyond: Innate Immune Cells As Regulators of Brain Development and Behavioral Function, Front. Immunol. 9 (2018) 698.

[5] M.-È. Tremblay, B. Stevens, A. Sierra, H. Wake, A. Bessis, A. Nimmerjahn, The role of microglia in the healthy brain, J. Neurosci. 31 (2011) 16064–16069.

[6] K. Sato, Effects of Microglia on Neurogenesis, Glia. 63 (2015) 1394–1405.

[7] C. Gemma, A.D. Bachstetter, The role of microglia in adult hippocampal neurogenesis, Front. Cell. Neurosci. 7 (2013) 229.

[8] A. Nieto-Quero, P. Chaves-Peña, L.J. Santín, M. Pérez-Martín, C. Pedraza, Do changes in microglial status underlie neurogenesis impairments and depressive-like behaviours induced by psychological stress? A systematic review in animal models, Neurobiology of Stress. 15 (2021) 100356.

[9] J. Lyu, X. Jiang, R.K. Leak, Y. Shi, X. Hu, J. Chen, Microglial Responses to Brain Injury and Disease: Functional Diversity and New Opportunities, Transl. Stroke Res. (2020). https://doi.org/10.1007/s12975-020-00857-2.

[10] S. Rosi, A polarizing view on posttraumatic brain injury inflammatory response, Brain Circ. 2 (2016) 126–128.

[11] M.W. Salter, B. Stevens, Microglia emerge as central players in brain disease, Nat. Med. 23 (2017) 1018–1027.

[12] K.M. Lenz, M.M. McCarthy, A starring role for microglia in brain sex differences, Neuroscientist. 21 (2015) 306–321.

[13] M. Bordeleau, M. Carrier, G.N. Luheshi, M.-È. Tremblay, Microglia along sex lines: From brain colonization, maturation and function, to implication in neurodevelopmental disorders, Semin. Cell Dev. Biol. 94 (2019) 152–163.

[14] E.A. Bordt, A.M. Ceasrine, S.D. Bilbo, Microglia and sexual differentiation of the developing brain: A focus on ontogeny and intrinsic factors, Glia. (2019). https://doi.org/ 10.1002/glia.23753.

[15] A.M.H. Young, N. Kumasaka, F. Calvert,…D.J. Gaffney, A map of transcriptional heterogeneity and regulatory variation in human microglia, Nat. Genet. 53 (2021) 861–868.

[16] R. Hanamsagar, M.D. Alter, C.S. Block, H. Sullivan, J.L. Bolton, S.D. Bilbo, Generation of a microglial developmental index in mice and in humans reveals a sex difference in maturation and immune reactivity, Glia. 66 (2018) 1504–1520.

[17] J.M. Schwarz, P.W. Sholar, S.D. Bilbo, Sex differences in microglial colonization of the developing rat brain, J. Neurochem. 120 (2012) 948–963.

[18] I. Kim, L.M. Mlsna, S. Yoon, B. Le, S. Yu, D. Xu, S. Koh, A postnatal peak in microglial development in the mouse hippocampus is correlated with heightened sensitivity to seizure triggers, Brain Behav. 5 (2015) e00403.

[19] L. Weinhard, U. Neniskyte, A. Vadisiute, G. di Bartolomei, N. Aygün, L. Riviere, F. Zonfrillo, S. Dymecki, C. Gross, Sexual dimorphism of microglia and synapses during mouse postnatal development, Dev. Neurobiol. 78 (2018) 618–626.

[20] L.H. Nelson, S. Warden, K.M. Lenz, Sex differences in microglial phagocytosis in the neonatal hippocampus, Brain Behav. Immun. 64 (2017) 11–22.

[21] B.D. Semple, K. Blomgren, K. Gimlin, D.M. Ferriero, L.J. Noble-Haeusslein, Brain development in rodents and humans: Identifying benchmarks of maturation and vulnerability to injury across species, Prog. Neurobiol. 106-107 (2013) 1–16.
[22] P.R. Mouton, J.M. Long, D.-L. Lei, V. Howard, M. Jucker, M.E. Calhoun, D.K. Ingram, Age and gender effects on microglia and astrocyte numbers in brains of mice, Brain Res. 956 (2002) 30–35.
[23] L.H. Nelson, P. Peketi, K.M. Lenz, Microglia Regulate Cell Genesis in a Sex-dependent Manner in the Neonatal Hippocampus, Neuroscience. (2020). https://doi.org/10.1016/j.neuroscience.2020.10.009.
[24] K.M. Lawrence, P.E. McGovern, A. Mejaddam, A.C. Rossidis, H. Baumgarten, A.G. Kim, J.B. Grinspan, D.J. Licht, E. Radaelli, J. Rychik, W.H. Peranteau, M.G. Davey, A.W. Flake, J.W. Gaynor, Prenatal hypoxemia alters microglial morphology in fetal sheep, J. Thorac. Cardiovasc. Surg. (2019). https://doi.org/10.1016/j.jtcvs.2019.06.102.
[25] F.G. Ibanez, K. Picard, M. Bordeleau, K. Sharma, K. Bisht, M.-È. Tremblay, Immunofluorescence Staining Using IBA1 and TMEM119 for Microglial Density, Morphology and Peripheral Myeloid Cell Infiltration Analysis in Mouse Brain, JoVE (Journal of Visualized Experiments). (2019) e60510.
[26] N.P. du Sert, V. Hurst, A. Ahluwalia,…H. Wuerbel, The ARRIVE guidelines 2.0: updated guidelines for reporting animal research, BMJ Open Science. 4 (2020) e100115.
[27] S. Yun, R.P. Reynolds, I. Petrof, A. White, P.D. Rivera,... A.J. Eisch, Stimulation of entorhinal cortex-dentate gyrus circuitry is antidepressive, Nat. Med. 24 (2018) 658–666.
[28] D.C. Lagace, M.H. Donovan, N.A. DeCarolis, L.A. Farnbauch, S. Malhotra, O. Berton, E.J. Nestler, V. Krishnan, A.J. Eisch, Adult hippocampal neurogenesis is functionally important for stress-induced social avoidance, Proc. Natl. Acad. Sci. U. S. A. 107 (2010) 4436–4441.
[29] P.R. Mouton, Principles and practices of unbiased stereology: an introduction for bioscientists, JHUP, 2002.
[30] M.J. West, Basic Stereology for Biologists and Neuroscientists, Cold Spring Harbor, New York, 2012.
[31] H.J. Gundersen, E.B. Jensen, The efficiency of systematic sampling in stereology and its prediction, J. Microsc. 147 (1987) 229–263.
[32] B. Gómez-González, A. Escobar, Prenatal stress alters microglial development and distribution in postnatal rat brain, Acta Neuropathol. 119 (2010) 303–315.
[33] B.F. Osborne, A. Turano, J.I. Caulfield, J.M. Schwarz, Sex- and region-specific differences in microglia phenotype and characterization of the peripheral immune response following early-life infection in neonatal male and female rats, Neurosci. Lett. 692 (2019) 1–9.
[34] N. Stence, M. Waite, M.E. Dailey, Dynamics of microglial activation: a confocal time-lapse analysis in hippocampal slices, Glia. 33 (2001) 256–266.
[35] G.M. Rurak, S. Simard, M. Freitas-Andrade, B. Lacoste, F. Charih, A. Van Geel, J. Stead, B. Woodside, J.R. Green, G. Coppola, N. Salmaso, Sex differences in developmental patterns of neocortical astroglia: A mouse translatome database, Cell Rep. 38 (2022) 110310.
[36] R. Paolicelli, A. Sierra, B. Stevens, M.-E. Tremblay,... T. Wyss-Coray, Defining Microglial States and Nomenclature: A Roadmap to 2030, Papers.ssrn.com. (2022). https://doi.org/10.2139/ssrn.4065080.
[37] A.D. Greenhalgh, J.G. Zarruk, L.M. Healy, S.J. Baskar Jesudasan, P. Jhelum, C.K. Salmon, A. Formanek, M.V. Russo, J.P. Antel, D.B. McGavern, B.W. McColl, S. David, Peripherally derived macrophages modulate microglial function to reduce inflammation after CNS injury, PLOS Biology. 16 (2018) e2005264. https://doi.org/10.1371/journal.pbio.2005264.
[38] M.L. Bennett, F.C. Bennett, The influence of environment and origin on brain resident

macrophages and implications for therapy, Nat. Neurosci. 23 (2020) 157–166.
[39] M.L. Bennett, F.C. Bennett, S.A. Liddelow, B. Ajami, J.L. Zamanian, N.B. Fernhoff,…B.A. Barres, New tools for studying microglia in the mouse and human CNS, Proc. Natl. Acad. Sci. U. S. A. 113 (2016) E1738–46.

FIGURES

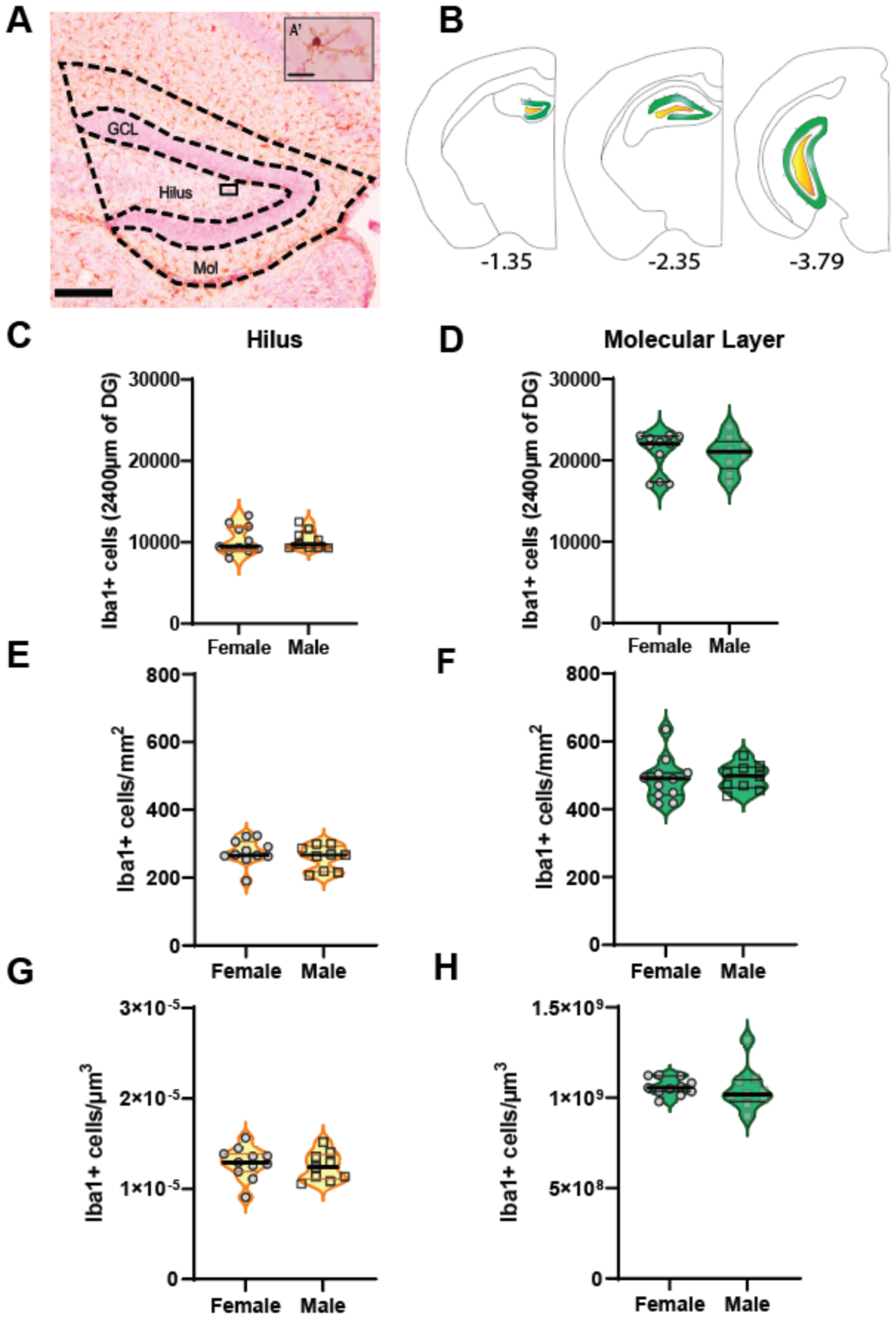
A
A'
GCL
Hilus
Mol
B
-1.35
-2.35
-3.79
C
Hilus
Iba1+ cells (2400µm of DG)
30000
20000
10000
0
Female
Male
D
Molecular Layer
Iba1+ cells (2400µm of DG)
30000
20000
10000
0
Female
Male
E
Iba1+ cells/mm2
800
600
400
200
0
Female
Male
F
Iba1+ cells/mm2
800
600
400
200
0
Female
Male
G
Iba1+ cells/µm3
3×10-5
2×10-5
1×10-5
0
Female
Male
H
Iba1+ cells/µm3
1.5×109
1×109
5×108
0
Female
Male

Figure 1. No sex differences in Iba1+ cell number, density, or volume in P10 mouse dentate gyrus via stereology. (A) P10 mouse dentate gyrus (DG) coronal brain section immunostained with anti-Iba1 antibody and counterstained with FastRed. Dotted lines display the regions (Hilus and Mol) in which the total Iba1 estimated population was generated by the optical fractionator probe. Granule Cell Layer (GCL) also shown but no cells were counted in this region. Scale bar=200µm. **(A')** Representative image of thin Iba1+ cell in the Hilus. Scale bar=25µm **(B)** Representative stereotaxic atlas plates of coronal sections from Bregma -1.35 to -3.79 showing the Hilus (green) and Mol (gold) where Iba1+ cells were counted. The total number Iba1+ cells were quantified in both the left and right hemispheres of P10 male and female mice within the anterior 2400µm of the DG, which included up to 10 hippocampal brain sections per mouse. **(C-D)** No sex difference in the total number of Iba1+ cells in the first 2400µm of the Hilus **(C)** or Mol **(D)**. **(E-F)** No sex difference in the total density of Iba1+ cells in the Hilus **(E)** or Mol **(F)**. **(G-H)** No sex difference in the total volume of Iba1+ cells in the Hilus **(G)** or Mol **(H)**.

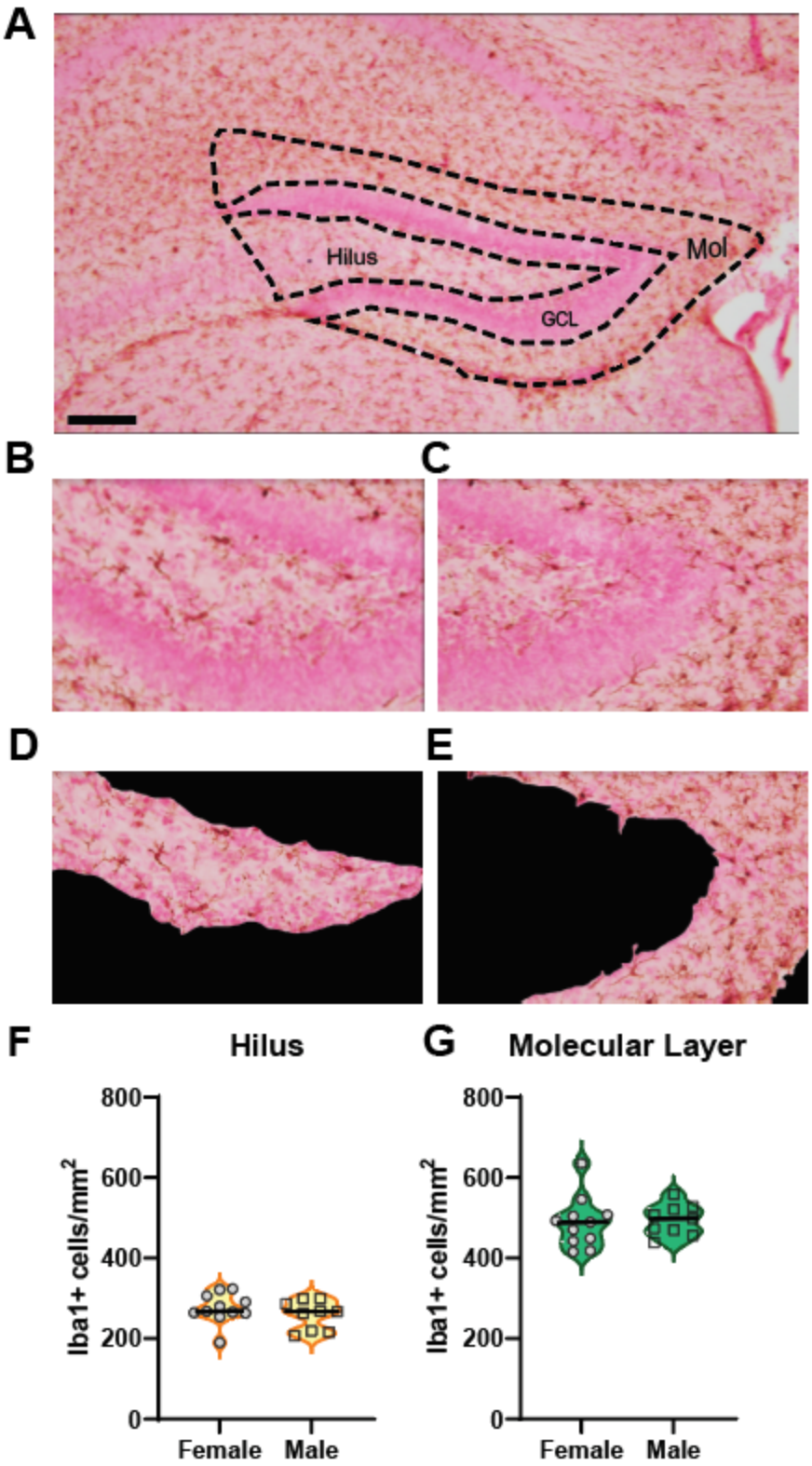

Figure 2: No sex differences in Iba1+ cell density via sampling in P10 mice Hilus and Mol. (A) Representative 10X photomicrograph of anterior Hilus and anterior Mol where cell density of Iba1+ cells was quantified. **(B-D)** After photomicrographs were collected, a region of interest (ROI) was drawn on each image using ImageJ. Surrounding areas were shaded out so only Iba1+ cells in the Hilus **(D)** or Mol **(E)** were counted. **(F-G)** No sex difference in the density of Iba1+ cells in the anterior Hilus **(F)** or anterior Mol **(G)**.

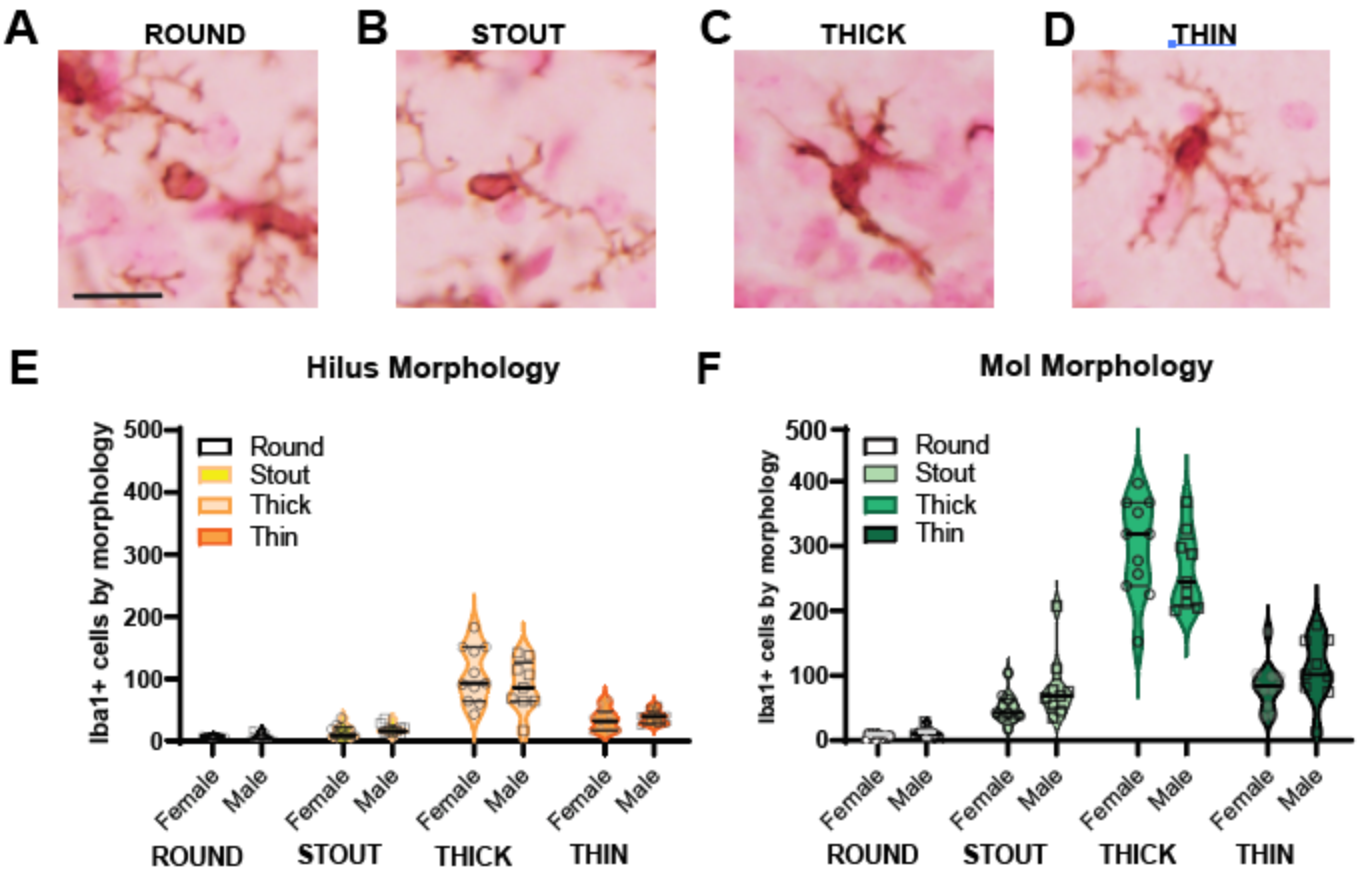

Figure 3. No sex difference in total number of Iba1+ cells by morphological type in mouse P10 Hilus and Mol. (A-D) Classification of Iba1+ cell morphology in mouse P10 hippocampal Dentate Gyrus. **(A)** Round (round-ish soma, no processes), **(B)** Stout (round-ish soma, short process), **(C)** Thick (irregular soma with few, thick processes), and **(D)** Thin (irregular soma with multiple thin processes). **(E-F)** Number of Iba1+ cells by morphological type in one section of mouse P10 Hilus and Mol. The percentage of Iba1+ cells in each morphology category in male and female mice generated by cell density data was multiplied by the total number of Iba1+ cells generated by stereology data in the **(E)** Hilus and **(F)** Mol. In each subregion, Iba1+ Thick and Thin cells were most prevalent, while Iba1+ Round and Stout cells were far more rare. Iba1+ Round cells were sometimes absent altogether. No significant difference by sex with regards to Iba1+ cell morphology classification in either region. Scale bar = 25um and applies to **(A-D)**